Astron. Astrophys. 314, 303–311 (1996)

ASTRONOMY AND ASTROPHYSICS

Transport of superthermal electrons in coronal loops and U(N)-type solar radio bursts

M. Karlický[1], G. Mann[2], and H. Aurass[2]

[1] Astronomical Institute of the Academy of Sciences of Czech Republic, 251 65 Ondřejov, Czech Republic
[2] Astrophysikalisches Institut Potsdam, Observatorium für solare Radioastronomie, Telegrafenberg A31, D-14473 Potsdam, Germany

Received 20 July 1995 / Accepted 19 December 1995

Abstract. Electron beams travelling with about 1/3 of the velocity of light along closed coronal loops can manifest themselves in decimeter and meter wave solar type U or U(N) radio bursts. Using a 1-D test particle model, we study trajectories of superthermal electrons in coronal loops with the aim of understanding recently published detailed radio spectral and imaging data about type U(N) bursts. The computations are carried out in a static semi-circular loop of 1 solar radius length. For modeling transport processes Coulomb collisions, mirroring of electrons in the loop magnetic field, and scattering in zones of enhanced whistler wave turbulence are taken into account. The formation of a finite zone of enhanced whistler turbulence in the loop top is consistently explained by the properties of loss-cone instability of a weak preexisting energetic particle component. In a model run initially electrons are injected upwards along the loop axis in one leg. Scanning the trajectories of electrons through the loop and representing them in space vs time and plasma frequency vs time plots, respectively, we get synthetic radio source distributions and radio spectra. The results can be analyzed in dependence on loop and particle parameters including the strength of whistler turbulence. Thus, we are able to model the essential aspects of observed U(N) bursts. We find that in a zone of sufficiently strong whistler turbulence near the loop top the initial electron beam is splitted up into two beams propagating from the top back and forward into both loop legs. Thus two widely separated radio sources brighten during the descending branch of U burst spectra. Moreover, we find that U(N) type radio bursts can be excited not only due to mirroring but also by scattering of electrons in whistler turbulence near a leg of the loop. For demonstrating the strength of the present model a simulation of an observed U(N) burst (February 23, 1993) is given.

Key words: hydrodynamics – Sun: flares; radio radiation; particle emission

Send offprint requests to: Marian Karlický

1. Introduction

During the flare process, but also during hours or even days outside flares (Klein 1994) stored magnetic energy is transformed into thermal energy, i.e., heating, and kinetic energy of highly energetic particles. These high energy particles can be trapped in closed magnetic field structures – the coronal loops – which are a main structural feature of the solar corona visible in different spectral ranges. Trapped particles are revealed e.g. by the emission of solar meter wave radio continua. On the other hand, during the flare process electron beams can be injected in coronal magnetic field structures. The beams can travel along open as well as along closed magnetic field lines. In radio spectra, they appear as type III and type U bursts, respectively.

Beam-driven fast drift bursts are a basic element in decimeter and meter wave solar radio burst spectral patterns and, moreover, the only more or less well understood type of solar radio bursts (Suzuki et al. 1985; Raoult et al. 1990; Vlahos & Raoult 1995). They provide a diagnostic tool for studying particle acceleration, injection and propagation in the solar corona. The appearance of the drift burst radio spectrogram reveals particle beams propagating toward regions of lower density along open field lines of the coronal magnetic field (type III bursts); propagation toward larger densities yields "reverse" drift bursts. Type U bursts show up in the dynamic spectrogram as a type III like rising branch that turns over into a descending (reverse drift) branch (e.g. Suzuki et al. 1985; see Fig. 8A of the present paper, too). Unlike the more frequent type III bursts, type U generating beams are thought to propagate in closed coronal structures, both in active region loops and in loops interconnecting two active regions. Occasionally a type U burst is followed by a new rising branch, forming a burst spectrum reminding the letter "N". Such bursts are called type N (Caroubalos et al. 1987; Hillaris et al. 1988). Here, we use for U bursts followed by an N branch in the spectrum the term U(N) bursts.

Recently, improved spectrographic and imaging observations have been used to study the detailed spectral-time and source structure of type U bursts thus providing a key for studying the beam dynamics respectively the plasma and field parameters during particle propagation in closed magnetic plasma

loops (Klein & Aurass 1993; Aurass & Klein 1995). A characteristic spatial double source structure during the descending branch of some type U burst spectra deserves for special attention.

In this paper we present a numerical model to simulate some of the processes leading to the emission of type U(N) bursts in the solar corona. We use a one-dimensional code to face test particles with Coulomb collisional scattering, magnetic mirroring and scattering at whistler wave turbulence along a part of the propagation path. Firstly, the general properties of our model are dealt with. We check that a zone of enhanced whistler wave turbulence at the loop top is not improbable for the present parameter range and a loss-cone distribution of a preexisting weak energetic particle population in the loop. Eventually, we explain the observed spatial double structure of some type U burst sources by electron scattering in a whistler turbulence zone near the loop top. Finally, for a special case (an U(N) burst on February 23, 1993; Fig. 8) the simulation is exemplified.

2. The numerical model

In the present study we use a 1-D test particle model (see also Karlický 1993; Karlický & Hénoux 1993), in which the trajectories of numerical electrons can be computed in a static coronal loop. Except where expressed explicitly throughout the paper we use the c.g.s. system of units. We consider a 1-D semicircular magnetic loop of the length of 1 solar radius which corresponds to 6001 numerical space grids. The total hydrogen density, temperature and magnetic field profiles can be prescribed in this model in dependence on the problem under study. Our aim is to apply the model to type U radio bursts. Therefore, we have chosen the model parameters as presented in Fig. 1: the density in the loop is computed using the condition for the hydrostatic equilibrium for the temperature of $T = 10^4$ K in the chromosphere and for $T = 1.5 \times 10^6$ K in the corona. The density at the top of the loop has been taken in accordance with the $4 \times$ Newkirk density model (Newkirk 1961; Palmer 1974). The magnetic field $B(h)$ in the loop is assumed as being proportional to the power δ of the pressure (Zweibel & Haber 1983)

$$B(h) = B_{\rm top}(P(h)/P_{\rm top})^{\delta}, \tag{1}$$

where $P_{\rm top}$ and $B_{\rm top}$ are the pressure and magnetic field at the loop top, chosen here as $B_{\rm top} = 1$–10 G. The δ is varying in the interval from 0 to 2.

The trajectories of all numerical electrons in the loop are computed. During a time step Δt_p the position L of electrons with a velocity $v_{\|}$ parallel to the loop axis were changed as follows

$$L_{\rm new} = L_{\rm old} + v_{\|}\Delta t_p. \tag{2}$$

As concerns the energy losses and the pitch angle changes of individual electrons three effects are taken into consideration:

1. The energy losses and pitch angle scattering of electrons due to Coulomb collisions with the surrounding plasma are calculated by a Monte Carlo method as in the paper of Bai (1982)

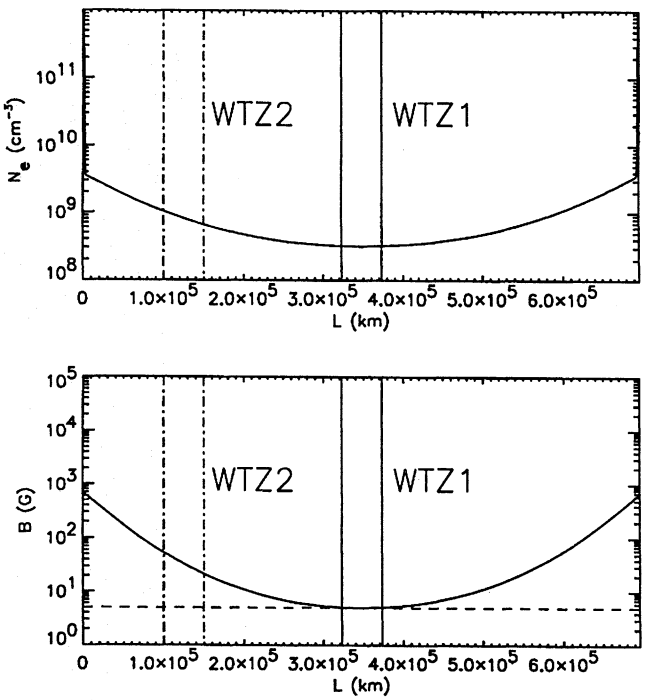

Fig. 1. Density and magnetic field profiles for testing our model. Concerning the magnetic field, see Eq. (1); $\delta = 2$ – continuous line; $\delta = 0$ – dashed line. WTZ1 and WTZ2 mean whistler turbulence zones, cf. Figs. 4, 5, and 6. The particle injection site is at $L = 600\,000$ km

(see also Karlický 1993; Karlický & Hénoux 1993), i.e., the following formulae were used:

$$\Delta E = \frac{4\pi n_e \Lambda e^4 L}{m_e v_0^2}, \tag{3}$$

$$\langle\theta^2\rangle = \frac{16\pi n_e e^4 \Lambda L}{\gamma_0^2 m_e^2 v_0^4}, \tag{4}$$

where E is the electron energy, $\langle\theta^2\rangle$ is the deflection angle of an electron passing a distance L, m_e is the electron mass, Λ is the Coulomb logarithm, n_e is the density of the surrounding plasma, γ_0 is the Lorentz factor, and v_0 is the initial electron velocity.

2. Magnetic mirroring effects are included similarly as in the paper by Karlický & Hénoux (1993, 1994) considering the conservation of the electron magnetic moment $p^2(1-\mu^2)/B$, where B is the magnetic field, p is the electron impuls and μ is the cosinus of electron pitch angle α.

3. Scattering at a zone of enhanced whistler turbulence (Melrose 1980) is taken into account along a certain part of the propagation path. For the computation of this scattering we use a Monte Carlo method as suggested by Miller & Ramaty (1989). We compute the coefficients of Fokker-Plank equation, i.e. the diffusion coefficient $D^w_{\mu\mu}$ as well as the coefficient of dynamic friction D^w_{μ} in the following form:

$$D^w_{\mu\mu} = \left(\frac{\pi^2 e}{m_e c} \left(\frac{2n}{n+1} \right) \frac{W_w^{\rm tot}}{B} \frac{1}{\gamma} \left(\frac{\beta\gamma}{1836\beta_a} \right)^{n-1} \right) \times |\mu|^{n-1} \left(1-\mu^2\right), \quad (5)$$

$$D^w_{\mu} = \left(\frac{\pi^2 e}{m_e c} \left(\frac{2n}{n+1} \right) \frac{W_w^{\rm tot}}{B} \frac{1}{\gamma} \left(\frac{\beta\gamma}{1836\beta_a} \right)^{n-1} \right) \times \mathrm{sign}\,(\mu) \left((n-1)\left(1-\mu^2\right) |\mu|^{n-2} - 2|\mu|^n\right), \quad (6)$$

where B is a magnetic field in G, γ is the Lorenz factor, β is a ratio between the electron velocity and the speed of light c, β_a is the ratio between Alfvén and light velocities, $W_w^{\rm tot}$ (erg cm^{-3}) is the total energy density of the whistler turbulence, and n is the index of the k^{-n} spectrum of the turbulence; n was taken equal to 7/3 (see Miller & Ramaty 1989). A change of pitch angle is computed according to Hua et al. (1989):

$$\Delta\mu = S(\langle(\Delta\mu)^2\rangle - \langle(\Delta\mu)\rangle^2)^{0.5} + \langle(\Delta\mu)\rangle, \quad (7)$$

where S is a random number having a normal distribution with a standard deviation of unity, $\langle(\Delta\mu)\rangle = D^w_\mu \Delta t$, and $\langle(\Delta\mu)^2\rangle = 2D^w_{\mu\mu}\Delta t$.

Special attention has to be devoted to the determination of the time step in calculating whistler wave scattering. The variance $\sigma^2 = \langle(\Delta\mu)^2\rangle - \langle(\Delta\mu)\rangle^2$ must be positive and the term $\langle(\Delta\mu)\rangle$ must be less than some critical value $\langle(\Delta\mu)\rangle_{\rm crit}$, which was chosen here as 0.1. We start using the time step $\Delta t_p = 10^{-2}$–10^{-3} s for the position change calculations and test these conditions. When the conditions are not fulfilled we decrease the scattering time step. Due to the singularity of the diffusion coefficient for $\mu = 1$ and $\mu = -1$, the electron scattering for the narrow cone corresponding to $0.98 \leq |\mu| \leq 1$ is neglected.

3. General results of the numerical modeling

In the following we stepwise adopt our model for studying the dominating effects for the formation of a type U(N) radio burst. The beam electrons are injected near one footpoint of the loop (see Figs. 2 to 6, part A) with the velocity $v = 10^{10}$ cm s^{-1}, and they propagate upwards as expected in the case of U type radio burst. We restrict the initial pitch angle to small values since only those pitch angles are involved in the two-stream instability. But these initial values are not chosen to be exactly zero in order to avoid singularities in the diffusion coefficients.

In Fig. 2 we give the simplest case when Coulomb collisions and a constant magnetic field along the loop are considered, only. In Fig. 2A the trajectories of 20 representative numerical electrons with initial pitch angle cosinus $\mu = -0.97$ are shown. Here, the sign minus only means that the electron beam is propagating in the negative direction of the length axis according to our choice of the system of reference (cf. Fig. 1). Assuming that electrons generate along their trajectories radio emission at the local plasma frequency, we can represent the trajectories in a frequency vs time plot as a synthetic radio spectrum (Fig. 2B) yielding the typical inverted U pattern.

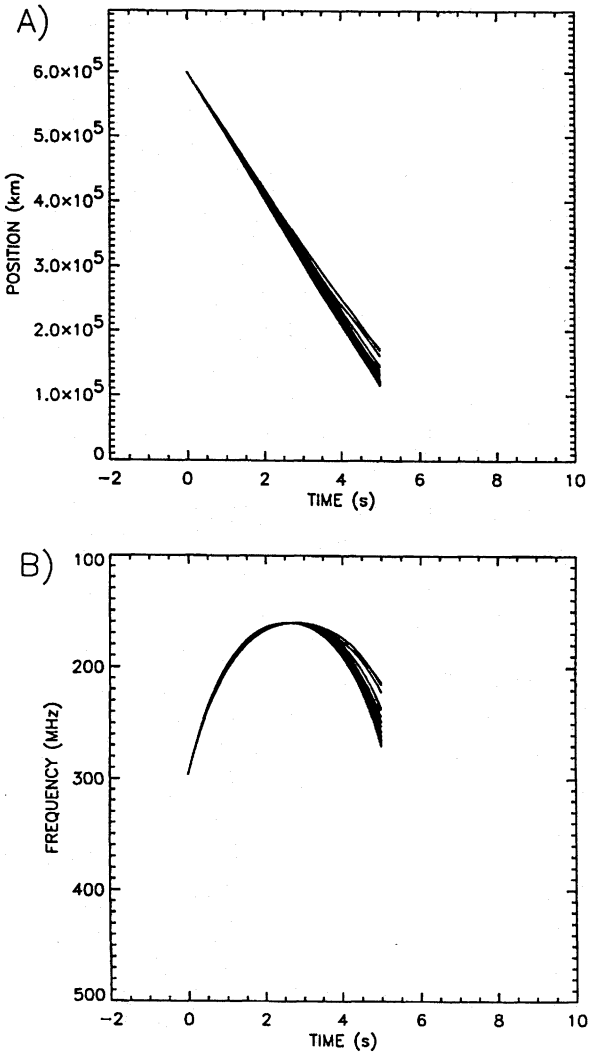

Fig. 2. The trajectories of 20 numerical electrons in the distance vs time (A) and the frequency vs time (B) plots for the case when only Coulomb collisions and constant magnetic field along the loop ($\delta = 0$) are considered. The initial μ for all electrons was -0.97

In Fig. 3 we model a U(N) type burst considering a converging magnetic field ($\delta = 2$). The initial μ is taken for all electrons equal to -0.80. The synthetic radio spectrum (Fig. 3B) really shows an additional somewhat diffuse branch (due to the mirrored particles) and reminds to the shape of the letter N.

Now we include a spatially limited zone of enhanced whistler wave turbulence at different locations in the model propagation path. Just this turbulence is able to scatter electrons very effectively in the energy range of beams generating U-bursts. For computing the results given in Figs. 4 and 5, the extent of this zone has been chosen as 50 000 km. Arguments for assuming a finite zone of enhanced whistler turbulence especially at the loop top are developed in Sect. 4. Mounting the whistler turbulent zone (WTZ1 in Fig. 1) at the loop top, computations have been carried out for two energy levels of the turbulence. We have assumed 10^{-6} and 10^{-5} erg cm^{-3}, respec-

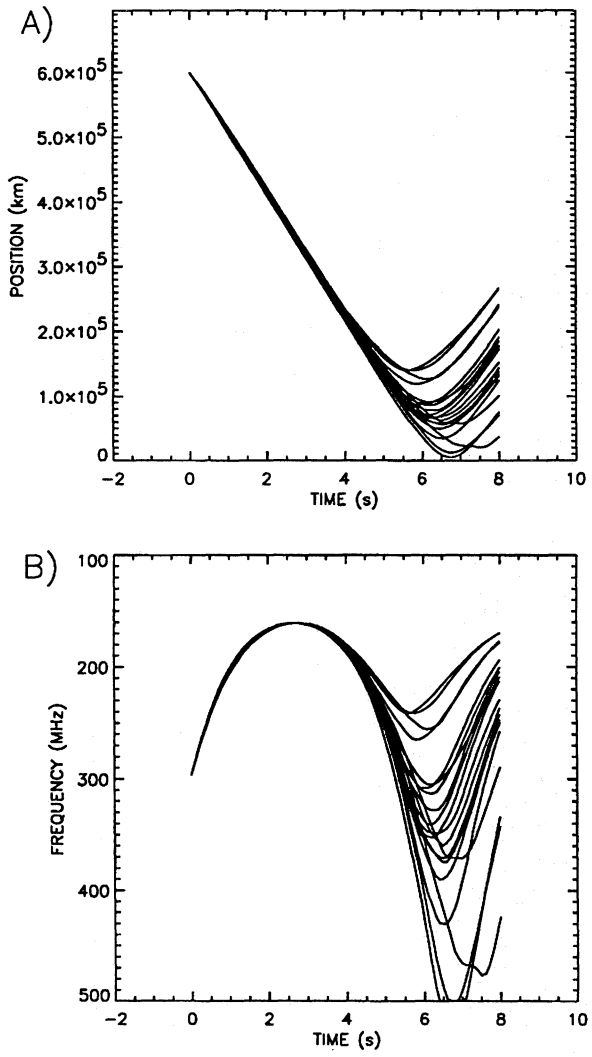

Fig. 3. The same as Fig. 2 but Coulomb collisions and mirroring are respected. The initial μ for all electrons was -0.80, and δ expressing the convergence of loop magnetic field was chosen as 2

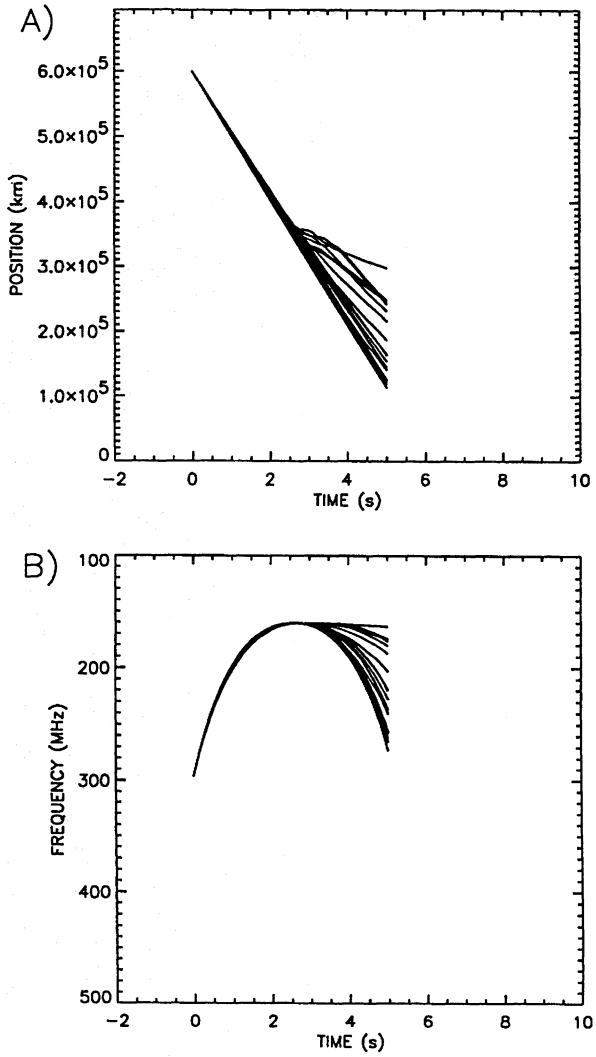

Fig. 4. The same as Fig. 2 but Coulomb collisions, mirroring and scattering of electrons at WTZ1 (cf. Fig. 1) are taken into account. The initial μ for all electrons was -0.97, δ expressing the convergence of loop magnetic field was 0.1, and the $W_w^{\rm tot}$ was chosen as 10^{-6} erg cm^{-3}

tively. A small convergence of the magnetic field corresponding to $\delta = 0.1$ has been assumed. While in the first case (Fig. 4A) no backmoving electrons are observed, in the case with higher whistler turbulence some electrons are backscattered from the turbulent region (see Fig. 5A).

That reminds to the fact (cf. Sect. 1) that the original beam (generating the ascending branch of the U burst spectrum) is splitted during the descending branch of the spectrum into two beams propagating toward opposite loop legs. Thus two spatially widely separated radio sources can be generated during this phase without any essential difference in the radio spectrum (compare Figs. 2B and 5B).

Finally, we demonstrate that U(N) bursts can be generated not only by magnetic mirroring as shown in Fig. 3, but also by scattering at a whistler turbulence zone above the mirror point and far away from the loop top. We assume that the turbulent region is situated between 1.0×10^5 km and 1.5×10^5 km (see Fig. 1, WTZ2). The energy level of the whistler turbulence has been chosen as 10^{-5} erg cm^{-3}. The model computation reveals that also in this case an additional branch forming an U(N) burst is evident in the synthetic radio spectrum.

4. On the localized whistler wave excitation

The whistler turbulence level of $W_w^{\rm tot} = 10^{-5}$ erg cm^{-3}, which is necessary to scatter a part of the electron beam back towards the incoming direction, can be established in the following way. The nonthermal energetic particles are produced not only during strong flares but also during the energetically weak, but much frequent flare-like processes (microflares). These electrons are trapped in coronal loops. Since the collision frequency $\nu_{\rm coll}$ (cf. Melrose 1980) is weak at the top of the loop, where the particle number density is essentially smaller than in the loop legs, the trapped electrons can mainly exist at the top of the loop for a

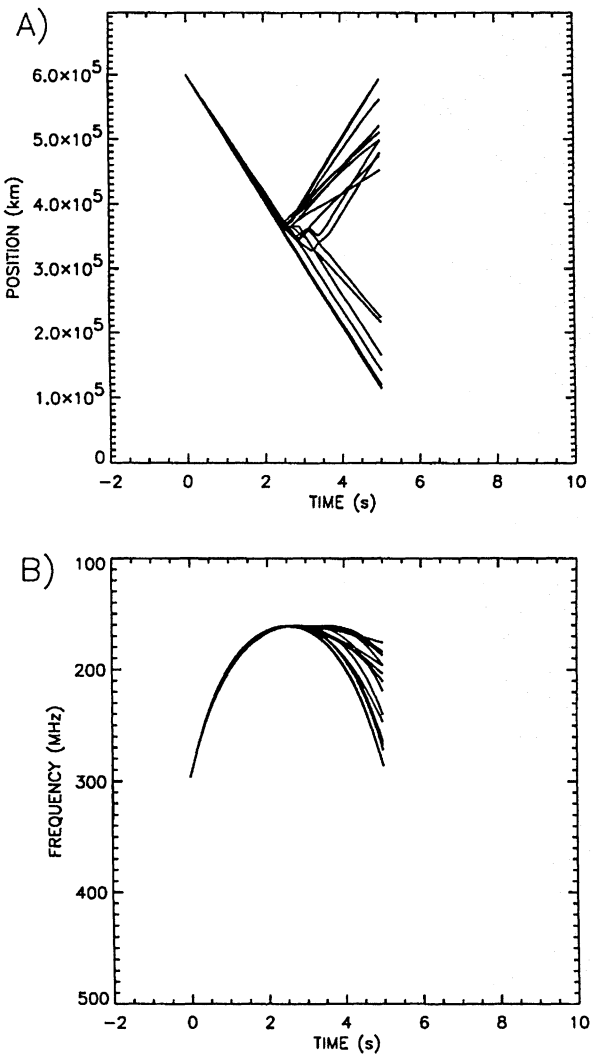

Fig. 5. The same as Fig. 4 with scattering at WTZ1 (cf. Fig. 1). The initial μ for all electrons was -0.97, δ expressing the convergence of loop magnetic field was 0.1, and the $W_w^{\rm tot}$ was chosen as 10^{-5} erg cm^{-3}

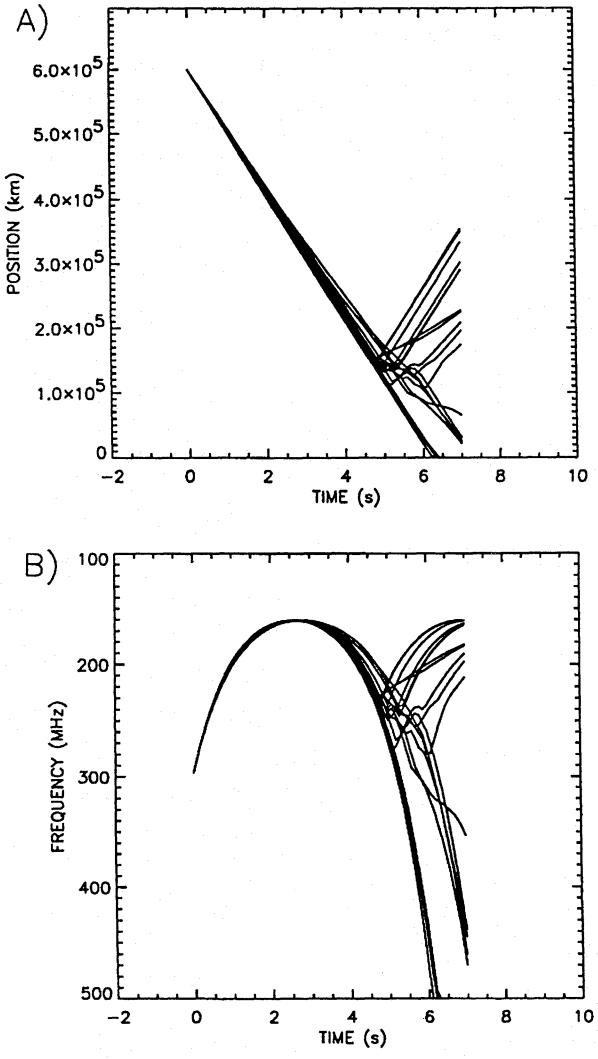

Fig. 6. The same as Fig. 4 but scattering at WTZ2 (cf. Fig. 1). Here is $\delta = 0$ and the initial μ for all electrons was -0.97; the $W_w^{\rm tot}$ was chosen as 10^{-5} erg cm^{-3}

relatively long time. We assume that this is the case just before the type U burst generation. These trapped electrons form a loss-cone distribution at the upper part of the loop. Such a distribution is unstable for exciting whistler waves (Kuijpers 1975; Berney & Benz 1978; Mann et al. 1989). In order to study the properties of the loss-cone instability the dispersion relation of whistler waves given by

$$\omega^2 = k^2c^2 + \pi \sum_j \frac{4\pi e^2}{m_j} \int_{-\infty}^{+\infty} dv_{\|} \times \int_0^{+\infty} dv_\perp v_\perp^2 \times \frac{(\omega - kv_{\|})\frac{\partial f_j}{\partial v_\perp} + kv_\perp \frac{\partial f_j}{\partial v_{\|}}}{(kv_{\|} - \omega + \epsilon_j \omega_{cj})} \quad (8)$$

(Krall & Trivelpiece 1973) must be numerically evaluated. Here, ω, k, c, e, and m_j denote the whistler frequency, the whistler wave number, the velocity of light, the elementary charge and the mass of the particle species j ($j = e$, electrons; $j = i$, protons), respectively. Furthermore ω_{cj} is the magnitude of the cyclotron frequency of the particle species j, i.e., $\epsilon_e = -1$ and $\epsilon_i = 1$. Here, a loss-cone distribution of energetic electrons superimposed upon a Maxwellian distribution of the thermal electrons and protons is considered, i.e.

$$f_e = f_{e0}(v) + f_{lc}(v), f_i = f_{i0}(v) \quad (9)$$

with

$$f_{j0} = \frac{N_0}{(2\pi v_{j0}^2)^{3/2}} \exp\left(-\frac{v^2}{2v_{j0}^2}\right), \quad (10)$$

and

$$f_{lc}(v) = \frac{N_{lc}}{(2\pi v_{lc}^2)^{3/2} \cos\alpha_{lc}} \times \Theta(v_\perp - v_{\|} \tan\alpha_{lc}) \exp\left(-\frac{v^2}{2v_{lc}^2}\right) \quad (11)$$

($v^2 = v_\parallel^2 + v_\perp^2$). Here, $v_\parallel$ and $v_\perp$ denote the components of the particle velocities parallel and perpendicular to the ambient magnetic field. Θ is the well-known step function, α_{lc} represents the loss-cone angle. v_{lc} is the mean velocity of the high energy electrons trapped within the loop. v_{j0} is the thermal speed of the particles of the species j, i.e., $v_{j0} = (k_B T/m_j)^{1/2}$ (k_B, Boltzmann's constant; T, temperature). Generally, the distribution functions are normalized to the particle number densities N_0 and N_{lc} of the thermal particles and the high energy electrons. Here, the high energy electrons are regarded as a minor component, i.e., $N_{lc} \ll N_0$.

At the 200 MHz level in the solar corona the following plasma parameters are usually found: particle number density $N = 5 \times 10^8\,\mathrm{cm}^{-3}$, magnetic field $B = 5\,\mathrm{G}$ and temperature $T = 10^6\,\mathrm{K}$. These parameters result in an electron cyclotron frequency $\omega_{ce} = 8.8 \times 10^7\,\mathrm{s}^{-1}$, a Debye length $\lambda_D = 0.30\,\mathrm{cm}$ and a collision frequency $\nu_{\mathrm{coll}} = 120\,\mathrm{Hz}$. The thermal level of whistler turbulence is given by $W^w_{\mathrm{therm}} \approx (2N\lambda_D^3)^{-1}$ (Krall & Trivelpiece 1973). Here, the wave energy density W^w is normalized to $2N k_B$ T, i.e., $W^w = |E_w|^2 / 16\pi N k_B T$ (E_w, amplitude of the electric field of the whistler wave). Thus, the energy density of the thermal whistler turbulence is found to be $W^w_{\mathrm{therm}} = 5.2 \times 10^{-9}\,\mathrm{erg\,cm}^{-3}$. Then, the required whistler turbulence level of $W^w_{\mathrm{tot}} = 10^{-5}\,\mathrm{erg\,cm}^{-3}$ is 2000 times the thermal level. Such a level can be excited by the above mentioned loss-cone instability. This should be done within a time period smaller than the collision time $\nu^{-1}_{\mathrm{coll}} = 0.01\,\mathrm{s}$. Thus, a time of whistler excitation of 0.005 s appears to be appropriate in order to provide the required level of whistler turbulence in the top of the loop. Because of $W^w_{\mathrm{tot}}/W^w_{\mathrm{therm}} = \exp(2\gamma_{\max} t)$ an increment $\gamma_{\max} = 756\,\mathrm{s}^{-1}$ is needed, i.e., $\gamma_{\max}/\omega_{ce} = 8.6 \times 10^{-6}$.

Figure 7 represents the result of the numerical evaluation of the dispersion relation (9) employing the distribution functions (10–12) using the parameters ω_{pe}/ω_{ce}=15, $N_0 = 5\times 10^8\,\mathrm{cm}^{-3}$, $T = 1 \times 10^6\,\mathrm{K}$, $N_{lc}/N_0 = 5 \times 10^{-6}$ and $v_{lc}/c = 0.33$. Here, ω_{pe} denotes the electron plasma frequency. The maximum increment $\gamma_{\max}$ normalized to the electron cyclotron frequency versus the loss-cone angle is depicted in Fig. 7. The above required increment, $\gamma_{\max}/\omega_{ce} = 8.6 \times 10^{-6}$, appears in regions with a loss-cone angle of about 60°. This loss-cone angle is established in a magnetic mirror with the very small mirror ratio of $B_{\mathrm{top}}/B_{\mathrm{mirror}} = 0.75$, i.e., $B_{\mathrm{mirror}} = 6.7\,\mathrm{G}$. Therefore, the loss-cone distribution function is extended only near the top of loop. Note, that in loop legs due to much higher collision frequency the superthermal electrons are not present before the type U burst generation. Thus the whistler turbulence is established only near the top of loop as was assumed in numerical simulations.

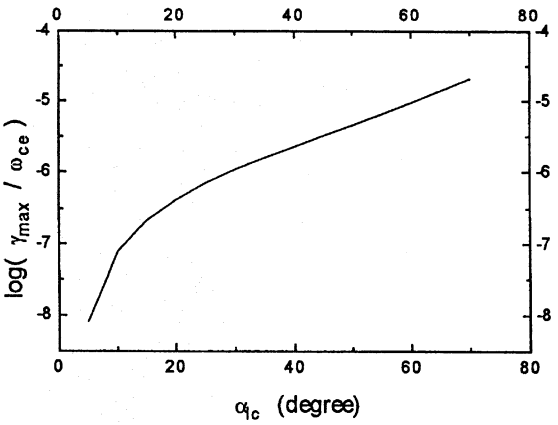

Fig. 7. Dependence of the maximum increment $\gamma_{\max}/\omega_{ce}$ on the loss-cone angle α_{lc} for the loss-cone instability (cf. Eqs. (9–12)) with parameters: $\omega_{pe}/\omega_{ce} = 15$, $N_o = 5 \times 10^8\,\mathrm{cm}^{-3}$, $T = 1 \times 10^6\,\mathrm{K}$, $N_{lc}/N_o = 5 \times 10^{-6}$, $v_{lc}/c = 0.33$

5. Model application to the U(N)-type radio burst of February 23, 1993

To demonstrate the strength of the present model we use it for simulating the U(N) radio burst observed on February 23, 1993 (cf. Aurass & Klein 1995, 1996).

Figure 8A shows the type U(N) burst spectrum (spectrometer of the Observatory of Solar Radioastronomy of the Astrophysikalisches Institut Potsdam in Tremsdorf) starting 10 min after a subflare in NOAA AR: 7432 (S16E20, Solar Geophysical Data). The main features of the radio source configuration are shown in the one-dimensional scans and the flux curves of the different subsources given in Fig. 8B (Nançay multifrequency radio heliograph of the Paris-Meudon Observatory, NRH). The gross source site pattern confirms the model of an electron beam propagating in a closed coronal loop: a brightening at a given site (the leg into which the beam is injected) during the rising branch in the spectrum (U_{up} in Fig. 8B) followed by a remote brightening during the descending branch in the spectrum (U_{down} in Fig. 8B). The time difference between ascending and descending branches of the U burst at 236.6 MHz is 2.7 s. The N branch of the spectrum (N in Fig. 8) occurs nearly at the site of the descending U branch source with 4.2 s time delay. Note that the N branch signature is more diffuse in comparison with the ascending U branch. In Fig. 8C the NRH radio source sites and their half widths are overlaid to the corresponding YOHKOH image. The burst sources are located near a large coronal soft X-ray loop (see Aurass & Klein 1996).

Looking more carefully to the details of Fig. 8B some additional weak sources become visible just in the beginning of the brightening of the main U descending and N branch sources. These faint brightenings are situated definitely at the source site of the rising U burst branch, this means near the beam injection site.

Now, let us try to simulate this observation. The length of the semi-circularly assumed loop is estimated to about 1 solar radius from radio heliographic and YOHKOH observations. Assuming radio emission at the fundamental of the plasma frequency the density at the turning point of the loop has been determined from the U burst top frequency. Given a prescribed range of particle speeds and the time scale of the radio observations, under the same assumption we can derive the plasma density at other points along the loop. Considering these geometrical and density

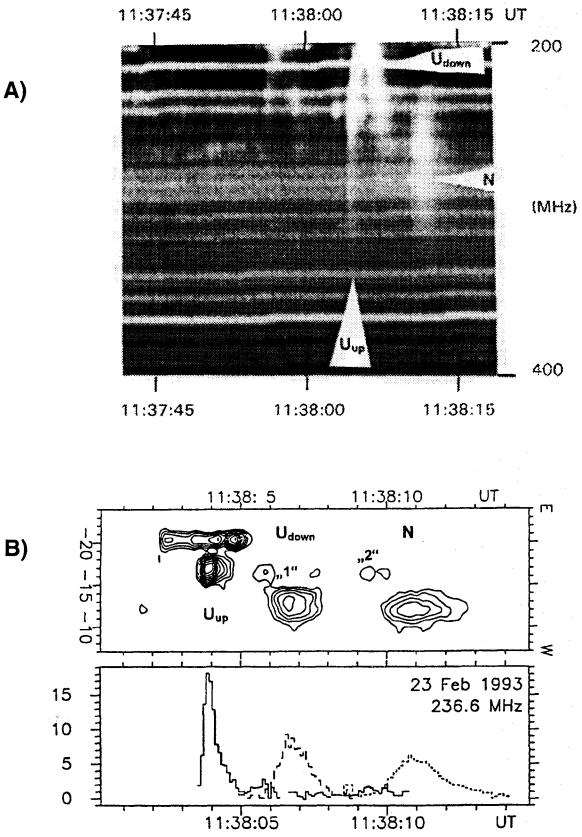

Fig. 8. The type U(N) solar radio burst on February 23, 1993 as observed by the 40–800 MHz spectrometer of Tremsdorf Observatory (A shows the 200–400 MHz range) and by the Nançay multifrequency radio heliograph of the Paris-Meudon Observatory, NRH (B, top, one-dimensional scan at 236.6 MHz; bottom the flux of the subsources in arbitrary units. Continuous line – ascending U burst branch; dashed line – descending U burst branch; dotted line – N burst branch). For designation "1" and "2" see Sect. 5 and Discussion and compare with Fig. 10A. C gives the YOHKOH soft X-ray image observed at 12:01:02 UT, overlaid are the 236.6 MHz NRH radio source positions and diameters (crosses with the same code like the flux curves in B). See Aurass & Klein (1996) for details

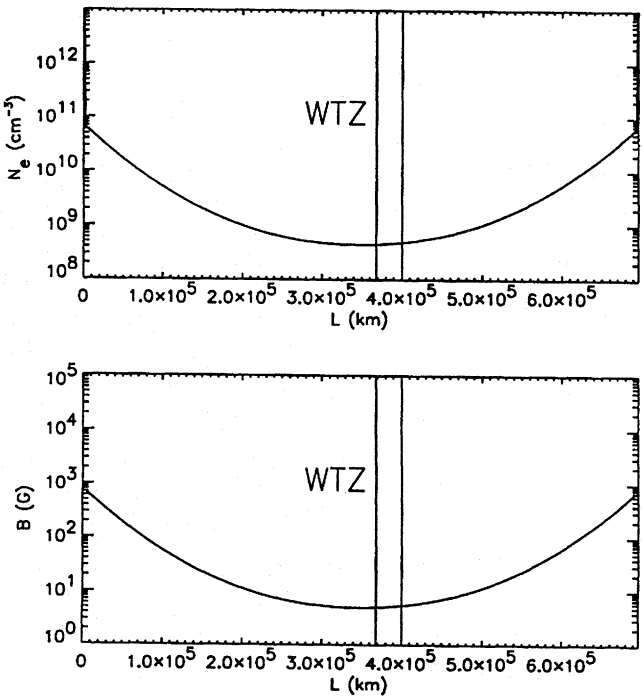

Fig. 9. Density and magnetic field profiles for fitting the February 23, 1993 observation. Concerning the magnetic field, see Eq. (1); $\delta = 1$. WTZ means whistler turbulence zone, cf. Fig. 10. The particle injection site is at $L = 545\,000$ km

aspects we build the density model which is presented in Fig. 9. The density height scale in this model is best fitted by a relatively low plasma temperature of 750 000 K. In varying the beam and the loop magnetic field parameters we fit the observed radio data (spectrogram, radio source site distribution, and timing) with our model. For an initial electron velocity of 10^{10} cm s^{-1}, an initial $\mu = -0.97$ and $\delta = 1$, and a plausible loop top magnetic field of $B = 5$ G the results shown in Fig. 10 are derived. Figure 10A shows the trajectories of 20 representative numerical electrons. Most of these electrons are propagating along the loop and are reflected by the magnetic mirror on the opposite side of the loop. These trajectories correspond to the gross characterictics of the observed U(N) radio burst (cf. Fig. 8B). For comparison with the observed radio spectrum (Fig. 8A) see Fig. 10B (the synthetic radio spectrum).

To explain the 2 weak subsources observed after the rising U burst branch at the injection site of the loop (cf. Fig. 8B) we refer to the whistler turbulence zone (see Fig. 9, WTZ) with an energy level $W_w^{tot} = 5 \times 10^{-6}$ erg cm^{-3}. In the present example, the whistler turbulence region must be near the loop top, but closer to the injection site as follows from the time sequence of the observed subsources (cf. Fig. 8B).

As evidenced by Fig. 10A, the zone of whistler turbulence backscatters some electrons. The backmoving electrons should form a faint reverse drift burst (the first weak subsource; "1" in Figs. 8B and 10A), some of these electrons are mirrored in the injection leg of the loop and just form also a secondary faint N burst branch (the second weak subsource, "2" in Figs. 8B

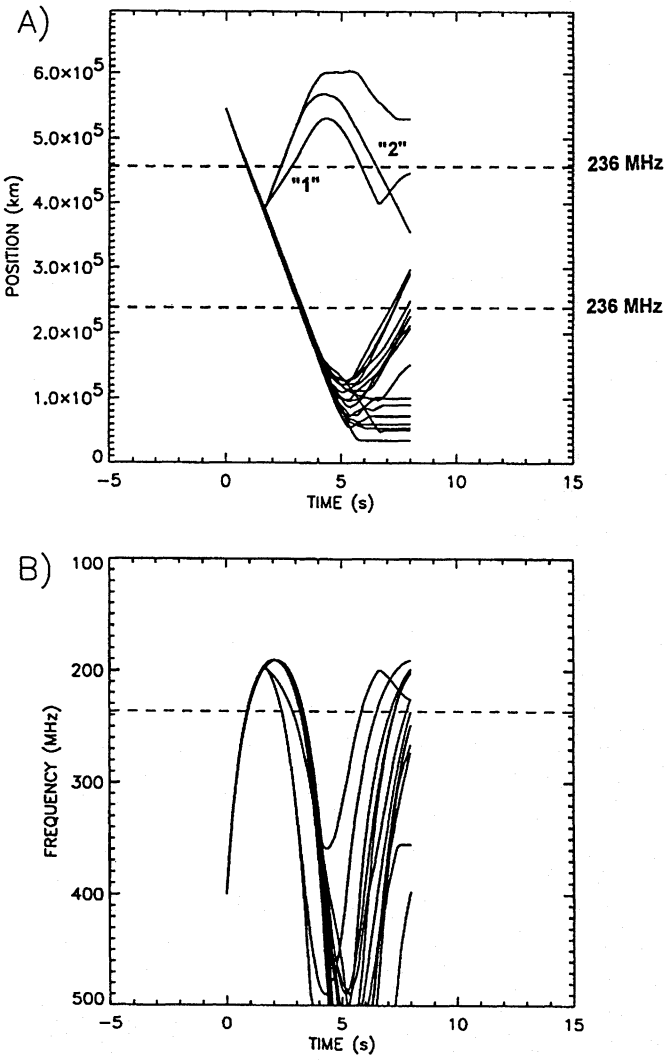

Fig. 10. The numerical simulation of the February 23, 1993 U(N) burst. The trajectories of 20 numerical electrons in the distance vs time (A) and the frequency vs time (B) plots for the case when Coulomb collisions, mirroring ($\delta = 1$) and scattering of electrons at whistler turbulence zone (WTZ, compare with Fig. 9) are considered. The initial μ for all electrons was -0.97, and the $W_w^{\rm tot}$ has been chosen as $5 \times 10^{-6}\,{\rm erg\,cm^{-3}}$. The dashed lines correspond to the frequency 236 MHz, the NRH observing frequency used in Fig. 8B. For designation "1" and "2" see Sects. 5 and 6, and compare with Fig. 8B

and 10A)! In the spectrum these faint additional N branches are covered by the stronger main U(N) burst spectral signature.

6. Discussion and conclusions

Using particle transport simulations we analyze in the present paper the effect of mirroring, scattering and Coulomb collisions on beam electrons and the resulting U(N) burst radio spectra. Further, we apply the model to the February 23, 1993 event.

We find the following main results:

1. Scattering of beam electrons at a zone of enhanced whistler wave turbulence near the loop top is important for understanding the observations. We have shown by a discussion of whistler wave excitation by the loss-cone instability that such turbulent zones can exist at the loop top. In considering this scattering we can explain the remarkable spatial splitting of some type U burst radio sources.

2. Scattering is efficient only for a sufficiently high energy level of the whistler turbulence and for an appropriate length of the turbulence zone. If the isotropization time due to scattering t_{is} is shorter than the electron passage time $t_{\rm pass} \approx v/L_{\rm zone}$, where v is the electron velocity and $L_{\rm zone}$ is the zone length , i.e. if

$$t_{is} = \left(\frac{\pi^2 e}{m_e c}\left(\frac{2n}{n+1}\right)\frac{W_w^{\rm tot}}{B}\frac{1}{\gamma}\left(\frac{\beta\gamma}{1836\beta_a}\right)^{n-1}\right)^{-1} < t_{\rm pass} \qquad (12)$$

is fulfilled then the whistler zone effectively scatters beam electrons. In our case, in agreement with the numerical results, it is fulfilled for whistler turbulence energy levels $W_w^{\rm tot}$ greater than $10^{-6}\,{\rm erg\,cm^{-3}}$. But if this zone is shorter or the whistler turbulence level is lower, then the zone is more transparent for transmitting electrons, i.e., less electrons are reflected.

3. Throughout the paper the test particle approach is used. The whistler turbulence is considered as fixed, therefore no self-consistent approach with wave-particle interactions, including Langmuir wave generation and quasi-linear relaxation has been taken into account. This is in accordance with the results of Hillaris et al. (1988) who showed that in the given coronal circumstances the effect of quasi-linear relaxation is strongly reduced (electrons are freely streaming).

4. Discussing the plasma frequency vs time plots (the synthetic radio spectra) we stress that curves which persist for some time on the same frequency correspond to electron trajectories with high pitch angles, i.e. to trajectories of electrons having a low velocity component parallel to the loop magnetic field. On the other hand, we remind that the type III and U bursts are generated due to the two-stream instability which needs field parallel electron beams. Therefore, the curves with low pitch angles, i.e. with high parallel velocities, are more important for the drift burst radio emission. This fact we respected in drawing Fig. 10. We have drawn there those trajectories of backscattered electrons which are able to explain the weak subsources mentioned in the previous Section and denoted by "1" and "2" in Fig. 8B and Fig. 10A. Once again we underline that in the present paper the transformation from particle trajectories into synthetic radio spectra has been done formally assuming fundamental plasma frequency emission.

5. We find that some U(N) bursts can be generated not only by mirroring in the convergent magnetic field but also by scattering of beam electrons by an assumed zone of enhanced whistler turbulence in a loop leg. This situation (Fig. 6) seems to us less probable in an undisturbed corona. Therefore, we accept mirroring of superthermal electrons as more probable explanation of the N branch of isolated U(N) bursts. But mirroring needs magnetic field convergence in the coronal part of the loop which is not supported by recent observational results (Strong & Bruner 1995).

6. We successfully applied our model to the U(N) burst of February 23, 1993. Of course we do not overestimate the diagnostic capability of our approach. Especially the model geometry must be improved.

Acknowledgements. We gratefully acknowledge Dr. K.-L. Klein for a critical reading of the paper and important hints for improving it. Furthermore, the authors express their thanks to the referee, Dr. Antoinette Raoult, for her helpful comments. One author (M.K.) would like to acknowledge the support of Deutsche Forschungsgemeinschaft (Grant No. 436TSE17/7/95) and Czech Academy of Sciences (Grant No. 303404). Further, he acknowledges the kind hospitality of the whole staff of the solar department during his stay at the Astrophysical Institute Potsdam. The authors are grateful to the YOHKOH community for their open data policy. Moreover, the authors express many thanks to H. Detlefs and P. Hackenberg for their help in solving several computing problems.

References

Aurass H., Klein K.L., 1995, Adv. Space Res. 17, 4/5, 269
Aurass H., Klein K.L., 1996, Spectrographic and imaging observations of solar type U radio bursts, A&A (accepted)
Bai T., 1982, ApJ 259, 341
Berney M., Benz A., 1978, A&A 65, 369
Caroubalos C., Poquérusse M., Bougeret J.L., Crépel R., 1987, ApJ 319, 503
Hillaris A., Alissandrakis C.E., Vlahos L., 1988, A&A 195, 301
Hua X.-M., Ramaty R., Lingenfelter R.E., 1989, ApJ 341, 516
Karlický M., 1993, Sol. Phys. 145, 137
Karlický M., Hénoux J.C., 1993, A&A 278, 627
Karlický M., Hénoux J.C., 1994, A&A 283, 202
Klein K.L., 1994, in: Lecture Notes on Physics Vol. 432, Springer, Berlin, 261
Klein K.L., Aurass H., 1993, Adv. Space Res. 13, 9, 295
Krall N.A., Trivelpiece A.W., 1973, Principles of Plasma Physics, McGraw-Hill, New York
Kuijpers J., 1975, Sol. Phys. 44, 173
Mann G., Baumgaertel K., Chernov G.P., Karlický M., 1989, Sol. Phys. 120, 383
Melrose D.B., 1980, Plasma Astrophysics. Gordon and Breach, New York
Miller J.A., Ramaty R., 1989, ApJ 344, 973
Newkirk G., 1961, ApJ 133, 983
Palmer I.D., 1974, Sol. Phys. 37, 443
Raoult A., Vlahos L., Mangeney A., 1990, A&A 233, 229
Strong K.T., Bruner M.E., 1995, Adv. Space Res. 17, 4/5, 179
Suzuki S., Dulk G.A., 1985, in: Solar Radiophysics, McLean D.J., Labrum N.R. (eds.). Cambridge University Press, Cambridge, 289
Vlahos L., Raoult A., 1995, A&A 296, 844
Zweibel E.G., Haber D., 1983 ApJ 264, 648